Intravascular Sensors to Assess Unstable Plaques and Their Compositions: A Review

Xing Xia[1†], Jimmy Zhang[2†], Gengxi Lu[3], Wen-Chi Lai[2], Sandeep K. Krishnan[4], Tzung K. Hsiai[5], Qifa Zhou[3], Anh H. Nguyen[1], and Hung Cao[1,2 *]

[†] *Equal contribution*

[1]Department of Electrical Engineering and Computer Science, University of California, Irvine, CA 92697

[2]Department of Biomedical Engineering, University of California, Irvine, CA 92697

[3]Department of Biomedical Engineering, University of Southern California, CA 90007

[4]Interventional Cardiology/Minimally Invasive Cardiac Surgery, Ascension St. John's, Tulsa, OK 74104

[5]Division of Cardiology, David Geffen School of Medicine, University of California, Los Angeles, CA

*Corresponding author:

Hung Cao, Ph.D.

Assistant Professor of Electrical and Biomedical Engineering

Henry Samueli School of Engineering, University of California, Irvine

Irvine, CA 92697, USA

E-mail: hungcao@uci.edu

Abstract

Atherosclerosis and its thrombotic complications plague developed countries. The rupture of vulnerable atherosclerotic plaques contributes to acute cardiovascular events and sudden cardiac deaths. Historically, coronary angiography has proved an invaluable tool for the detection and treatment of coronary stenoses that may cause myocardial ischemia; however, the method lacks the capacity to provide thorough information about properties of the lesion (i.e. whether it is lipid-rich, fibrotic, or calcified). Recent advances in electronics, biomaterials and microfabrication techniques have enabled novel multimodality catheters for the assessment of atherosclerotic plaques, such as the integration of intravascular ultrasound with photoacoustic microscopy or optical coherence tomography as well as the utilization of stretchable electrodes for electrochemical impedance spectroscopy. These technologies enable the identification of the complexity and composition of potentially unstable plaques as well as investigations of stenosis severity, plaque formation, and remodeling in both humans and studied animal models. However, real-time detection of vulnerable atherosclerotic lesions prepared for clinical trials remains an unmet challenge. In this context, this review highlights existing and newly-emerged intravascular sensors to assess unstable plaques and their compositions. Advantages and limitations, as well as further development and potential clinical applications, will be thoroughly discussed.

Keywords: *Intravascular sensors; Atherosclerosis; PET; Fractional flow reserve; Multi-frequency intravascular ultrasound.*

I. Introduction

Cardiovascular diseases, particularly coronary heart diseases, have been the leading cause of mortality in the world [1-7]. Rupture of unstable plaques is a cause of acute coronary syndromes, which are clinical manifestations of sudden reduction in perfusion and oxygenation to the myocardium, resulting in heart attacks. The vulnerability and susceptibility of atherosclerotic plaques have been investigated to reveal the relation with their compositions, the presence of associated inflammation, as well as the distributed mechanical stress [8-10]. For instance, the rupture of the thin-cap fibroatheroma's lipid-rich necrotic core due to high mechanical shear stress would release thrombogenic contents into the blood stream, resulting in occlusion [10, 11]. More than 18 million North Americans have atherosclerotic diseases, and both morbidity and mortality remain appreciable [12]. In the U.S., the prevalence of overt coronary artery disease is about 7 million with up to 2 million procedures performed annually [12, 13].

In hospitals, the gold-standard coronary angiography has been routinely employed to provide rapid assessment of the coronary vasculature to detect localized stenosis for treatment [14]. Although angiography is an invaluable tool to assess the entire coronary circulation system and to reveal localized stenosis, the two-dimensional (2D) visualization depicts only the lumen, thus possessing obvious limitations in structural and compositional analysis [14-17]. Therefore, a host of non-invasive three-dimensional (3D) imaging techniques have been developed and utilized for intravascular assessment, such as computed tomography (CT) angiography [18-20], magnetic resonance imaging (MRI) [21-23], single photon emission computed tomography (SPECT) [24-26], and positron emission tomography (PET) [27-29]. Nevertheless, these imaging tools still fail in characterizing and quantifying vulnerable plaques due to the deficiency in spatial and temporal resolution in coronary artery assessment [16]. During the last two decades, the development of catheter-based intravascular imaging techniques, such as intravascular ultrasound (IVUS) and intravascular optical coherence tomography (IVOCT), enabled not only 3D visualization but also quantification and characterization of atherosclerotic plaque burden. However, these techniques are invasive, and the information provided are localized. While IVUS can provide 70-200 μm

axial resolution, 200-400 μm lateral resolution, and 5-10 mm imaging depth using 10-60 MHz ultrasonic transducers, IVOCT technique possesses a much higher axial resolution (~10 μm), enabling fibrous-cap measurement, yet it only penetrates ~1.5 mm deep [16, 30]. This suggests that combining these two techniques would provide complementary results, where images would incorporate both high resolution detail near the artery lumen and the additional imaging depth needed for a more complete analysis.

During the past decade, we have attested tremendous applications of biosensors and biomedical devices in healthcare and biological investigations. The advances in micro- and nano-fabrication and electronics dovetailed with innovative biomaterials have enabled biocompatible miniaturized sensors and systems with significant improvement in sensitivity, selectivity, longevity, and reliability [31-34]. The existing platform of IVUS can be modified with additional miniaturized imaging modalities in order to provide better assessment of high-risk atherosclerotic plaques. Near infrared reflection spectroscopy (NIRS) has been used to realize the hybrid NIRS/IVUS catheter (by *Infraredx Inc.* – Burlington, MA), which has been proven to be capable of providing lipid assessment [11, 35-37]. However, NIRS cannot identify the relative location of the lipid core with respect to the lumen [11]. Previous studies reported the size of human coronary artery catheter with integrated IVUS and photoacoustic microscopy (PAM) is in a range of 1—4 mm, which provides a resolution of 19.6 μm, a 10-fold improvement over conventional devices [38, 39]. IVUS/PAM catheters are capable of identifying chemical specificity of the optical absorption of plaques [11, 17]. Furthermore, IVUS/PAM imaging could be combined with photothermal therapy (PPTT), which is a potential tool to treat specific atherosclerotic plaques via a local delivery of gold nanoparticles [17, 40, 41]. Using a nontraditional approach, Baer *et al.* developed a millimeter wave-based catheter for differentiation of atherosclerotic plaques by analyzing the scattering parameters (S-parameters) of a two-port configuration using 2 miniaturized antennas located on the tip of the catheter [42, 43]. While the method seemed promising, it has not been validated in animal models nor compared with existing means.

In the past several years, our team has developed several generations of flexible and stretchable intravascular microsensors to investigate pre-atherogenic lesions associated with oxidative stress in high-cholesterol-diet New Zealand White (NZW) rabbits using electrochemical impedance spectroscopy (EIS) [44-50]. We have been successful in linking oxidized low density lipoprotein (oxLDL) on vessel walls with distinct EIS signals [48]. For instance, oxLDL and foam cells infiltrating in the subendothelial layer has resulted in elevated frequency-dependent EIS [48]. The application of EIS strategy was also further employed to detect oxLDL-rich fibroatheroma using explants of human coronary, carotid, and femoral arteries [46]. The results were correlated with 60 MHz IVUS and oxLDL staining [49]. Recently, we have proposed and successfully developed an integrated catheter with both IVUS imaging and EIS, aiming to assess mechanically unstable plaques when patients are undergoing diagnostic angiogram or primary coronary intervention [51]. The experimental results with NZW rabbits demonstrated that topographic and EIS detection of oxLDL-laden plaques exhibited enhancement over the results seen in EIS alone. Furthermore, procedure time and X-ray exposure would be reduced when our newly developed device is clinically deployed.

In the next sections of this review paper, several important approaches for intravascular assessment of high-risk lesions will be presented and discussed. In detail, PET and ^{18}F-Sodium Fluoride (NaF) will be given in Section II, fraction flow reserve (FFR) and microelectromechanical systems (MEMS) will be addressed in Section III, and dual-frequency and high-frequency IVUS will be reviewed in Section IV. In-depth discussions about EIS, combined means, limitations and advantages, as well as future trends will follow.

II. PET and ^{18}F-Sodium Fluoride (NaF)

There is an unmet need for noninvasive imaging tools that can go beyond anatomic imaging to identify prospective culprit lesions in coronary arteries [52]. Molecular imaging is thus positioned to play a key role in the *a priori* identification of vulnerable plaques. Several well-known processes are involved in atherosclerotic plaque progression, including inflammation, calcification, and neovascularization. These

processes are well suited to evaluation using molecular imaging. The current armamentarium of molecular imaging agents includes ligands for receptors on macrophages and neovascular endothelial cells, and substrates for chemical reactions that selectively occur in vulnerable plaque, labeled with radioisotopes or paramagnetic agents. Imaging of molecular radiopharmaceutical agents is done via many routes, but we will focus on PET-CT scanning here. (PET/CT) imaging of atherosclerosis using ^{18}F-sodium fluoride (^{18}F-NaF) shows the potential to determine pathologically high-risk nascent microcalcification [53]. PET-CT scanning is based on the principle that when positrons and electrons collide, they annihilate each other and generate a unique radiation signal that can be detected within the body in a safe, efficient, and non-invasive manner. A variety of positron-emitting radiotracers can be designed to target a specific disease or process of interest that can then be detected by the PET scanner. The resulting PET image is then fused with detailed structural information from simultaneously obtained CT images to provide a map of activity within the body, shown in **Figure 1**. Whilst combined PET-CT imaging has been widely used in cancer patients, the complexities of correcting for motion meant that it has only recently become applicable to detect cardiac disease. The precise molecular binding mechanism of ^{18}F-NaF vascular uptake has been determined by electron microscope, autoradiography, histology, preclinical and clinical PET/CT [53].

A potential target for molecular imaging of vulnerable plaques is vascular calcification—long considered a hallmark of atherosclerosis with high affinity, selectivity, and specificity [53, 54]. Vascular calcification is believed to occur in response to hypoxia [55], necrosis [56] , and chronic inflammation [57]. It has been linked with macrophage burden and neovascularization. From biomechanical analysis, it is known that the presence of calcification on a distensible surface, such as the vascular endothelium, induces a compliance mismatch of the vessel, making it prone to rupture, especially at the tissue-calcium interface. The risk of rupture increases when multiple calcium deposits are present in close proximity [58]. As the number of calcium deposits grows, the vessel becomes more vulnerable due to the increase in points of tension and areas where the plaque is likely to rupture. ^{18}F-NaF PET/CT imaging can clearly identify which areas of macro- and microcalcification that are free of invasion in microcalcification in active unstable

atherosclerosis detection. The use of ^{18}F-NaF may open new interests to studying therapeutics for vascular calcification. However, as the "spotty" calcification coalesces, the larger nodules become more stable as the surface area exposed to vascular shear stresses decreases. Thus, there is a biphasic relationship of spotty calcification and plaque vulnerability [58-60].

Currently, ^{18}F sodium fluoride (^{18}F-NaF) is the only available imaging tracer known to identify active mineral formation arrays (MFA)—a key feature of vulnerable atheroma [61]. In bone, fluoride binding to areas of calcification is mediated via a chemical reaction with hydroxyapatite, a crystalline structure that is also the main component of vascular mineralization. It was hypothesized that MFA and hydroxyapatite would be abundantly found at the site of vulnerable, active plaque.

Irkle and colleagues demonstrated that ^{18}F-NaF preferentially binds microcalcification because the extent of fluoride adsorption depends on the surface area of the mineral. The complex structure of microcalcification allows more binding of fluoride ions as compared to the relatively flat surface found in macrocalcification. The presence of non-radioactive fluoride within calcified and soft tissue areas of carotid endarterectomy specimens was measured via electron microscopy, and microcalcifications contained greater levels of fluoride relative to macrocalcifications [59].

In a prospective study of 80 patients with myocardial infarction and stable angina, Joshi *et al.* showed that ^{18}F-NaF identified vulnerable coronary lesions that were implicated in causing the infarction. The results indicated a tissue to background ratio of 1.6 (1.40-2.25) vs 1.24 (1.06-1.38; $p<0.0001$) for non-culprit coronary plaques. ^{18}F-NaF uptake also correlated with 20 MHz IVUS findings of microcalcification, necrotic core and positive remodeling. This study has generated enthusiasm for using ^{18}F-NaF as a potentially useful tracer for identifying vulnerable plaques at risk of rupture and in identifying so-called "vulnerable patients" [62].

The mechanism for the identification of recently ruptured plaque has been hypothesized. It is known that macrophages have the capacity to transform mesenchymal cells to an osteoblastic phenotype, and it is likely that microcalcification may be mediated in large part due to the resident macrophages in highly

inflamed plaque. ^{18}F-NaF may therefore allow identification of plaques which have high inflammation and increased metabolic activity reflected by high rates of hydroxyapatite deposition. This may at least partially explain why ^{18}F-NaF may be superior than ^{18}F-FDG for identification of vulnerable plaque. Additionally, the myocardium does not extract ^{18}F-NaF for its metabolic needs; and therefore, patients do not have to consume a special diet prior to the scan to suppress background uptake. This provides a promising future for research with ^{18}F-NaF as an imaging tracer of plaque vulnerability.

Nevertheless, PET imaging with ^{18}F-NaF poses several challenges. This method requires long examination, radiation exposure, and invasive technique. Localization of uptake may be difficult due to the small size of the coronary arteries and superimposed cardiac and respiratory motion. Additionally, precise anatomical localization is further complicated due to relatively low uptake in the surrounding organs. Furthermore, cardiac and respiratory motion during a 30-minute scan significantly blurs the PET signal, necessitating co-registration with coronary computed tomography angiography (CCTA). In **Figure 2,** we show an example of an ^{18}F-NaF case acquired at our institution. To partially mitigate motion of the coronaries, end-diastolic imaging has been performed utilizing only 25% of the PET scan [62], but at the expense of increased image noise. Recently, Rubeaux *et al.* have shown that computational motion correction techniques can overcome these challenges [63]. ^{18}F-NaF is shaping up to be a promising molecular imaging agent.

III. Fractional flow reserve and microelectromechanical systems

Fractional flow reserve (FFR), defined as the ratio of maximum flow in the presence of a stenosis to normal maximum flow, is the gold-standard invasive method for assessing the hemodynamic significance in coronary lesions and coronary plaques associated with ischemia [64]. Basically, FFR is independent from all changes in the systemic blood pressure, heart rate, and conditions that can increase the base-line myocardial flow [65].

FFR was used to intervene to collateral blood supply to maximal myocardial perfusion [66]. In addition to established FFR technologies, three new options are emerging that may simplify FFR use,

eliminate adenosine, and change how patients are assessed both invasively and noninvasively. The association between composition, sizes of plaque, and lesion-specific ischemia were reported through coronary plaque quantification and FFR [64, 67]. Integrated in the FFR monitoring device, the electric or optical fiber pressure sensor is the most significant sensing element to provide clinical measurements in coronary artery disease (CAD) [68, 69]. Although FFR have clear clinical benefits, it is still not used in many patients because of its costs, procedural times, and the use of adenosine as a stressor agent, which can be unfamiliar to the patients [70]. Therefore, the new established FFR technologies may simplify FFR use such as adenosine elimination and changing assessment between invasive and noninvasive methods for patients. In this system, a pressure sensor integrated in a catheter is used to measure and calculate the ratio between the coronary pressure distal to the stenosis and the aortic pressure during hyperemia, occurring after ventricle contraction [71, 72]. In patients with multiple coronary lesions, FFR can be applied to identify which lesion is the main cause to ischemia, which may contribute to less use of stents implanted, leaving less adverse lesions alone. The reduction of stents based on FFR measurement may increase the patient's chances of less stent-related complications of in-stent restenosis and stent thrombosis [73].

Usually, an FFR value lower than 0.75-0.8 indicates a plaque that significantly obstructs blood flow in the vessel [74]. Conventionally, after the intracoronary administration of adenosine to stimulate hyperemia, a pressure guide wire is then directed towards the distal end of the plaque to measure the pressure [75]. While FFR has been documented as the gold standard for determining the functional significance of plaques in the coronary artery, there can be discrepancies due to the presence of certain measurement conditions [76]. When measuring FFR, maximum hyperemia must be induced to provide the most accurate readings for the pressures [77]. If hyperemia is not achieved, then the aortic pressure would be lower than normal, resulting in an increased FFR value. A way of ensuring hyperemia is by routinely administering adenosine during the procedure. Other concerns include the obstruction of blood flow by the catheter (as small as 0.36 mm) or dampening aortic pressures due to residual contrast found on the catheter [78]. Studies have also shown discrepancies when determining the specific cutoff values for determining

the functional significance of the plaques [79]. In a 2004 study involving 55 patients with left main coronary artery stenosis, the FFR cutoff value was determined to be 0.75 [80] . However, a 2008 study involving 3 patients with ambiguous results for left main coronary artery stenosis indicated that the cutoff value was not clear [81], acknowledging a "grey area" for diagnosis is present between 0.75 and 0.8 [82]. A possible reason for the presence of this grey area is the lack of standardization of FFR procedures across various studies [83]. Because studies were limited in sample size, various conditions might be overlooked, such as the nonrandomized samples or omission of certain disease types due to difficulty in measurement. Therefore, a large multi-center study incorporating the same methodology in measurement should be implemented to better understand correlations in FFR values.

Recently, microelectromechanical systems (MEMS) are widely applied in many areas due to the growing demands for elaborate millimeter-scale or even micrometer-scale sensors [84]. Some MEMS-based sensors have been proposed for the monitoring of flow properties and the measurement of fractional flow reserve, supported by a computational-fluid dynamic algorithm derived FFR 3D model for non-invasive coronary imaging [85]. Combined with CT scan, the system allows very well scanning the anatomical plaques with an 80 percent correlation compared to invasive FFR [86, 87]. The system provides a value that compares the arterial pressure downstream from the plaque (distal pressure) and the aortic pressure during hyperemia through the availability of accurate pressure-sensing [88]. Additionally, MEMS technology is critical in the development of FFR sensors. Because of the need to miniaturize the outer diameter catheter below the millimeter scale, FFR sensors require the high architecture level of MEMS to fit a pressure sensing system into the outer walls [71, 89]. However, maintaining flexibility for the catheter to track the arterial system can still be a challenge, such as the design of a flex layout that could wrap into a small structure needs the precision in fabrication processes.

The capacitive pressure sensor is one of the most developed and commonly used pressure sensors for FFR measurement because it works with high pressure sensitivity and low temperature [84]. Capacitive sensors are based on parallel plate capacitors. A simple structure of the capacitive pressure sensor is shown

in **Figure 3**. The upper diaphragm of the capacitive pressure sensor is distorted by external force, which leads to a change of capacitance between parallel plate capacitors. Recent studies reported an integration of a capacitive MEMS pressure sensor and an application-specific integrated circuit (ASIC) for intracorporeal physiological condition monitoring and coronary artery FFR measurements through piezo-electric coronary pressure wires [71, 90]. Recently, Yang *et al.* [91] designed a flexible, tunable, and ultrasensitive capacitive pressure sensor with micro-conformal graphene electrodes. The sensor was carefully fabricated by using different methods including the traditional polymethylmethacrylate (PMMA)-mediated transfer method, the ultraviolet-curable adhesive (UVA) mediated transfer method, and the micro-conformal transfer method. This approach improved the sensitivity of capacitive pressure sensors. By sandwiching the PDMS dielectric layer between the micro-structured graphene electrode and bottom electrode, the capacitive pressure sensors with their diameter 0.67 mm obtained high, tunable sensitivity, fast response speed, ultralow detection limit, high flexibility, and high stability [92].

Piezoresistive pressure sensors are also widely proposed for blood pressure measuring with low-cost sensor fabrication and either on-chip- or discrete read-out circuitry [93]. Moreover, the sensors were miniaturized, consisting of a 15 μm thick cantilever, two sensing beams, and four wiring beams to work in a triaxial force measurement sensor probe. The sensors are formed at the root of the cantilever and the sidewalls of the two sensing beams, which are able to measure triaxial forces with a minimum detectable force at the sub-micronewton level [94]. This design is further developed into the proof-mass mechanical structural design parameters of a tri-axial piezoresistive accelerometer for the plaque structure stress estimations, which is responsible for most myocardial infarctions [95]. The device would respond to the highest achievable sensitivity with a single proof-mass approach and achieve a very low error (<1%) for determining plaque regression and stabilization [96]. Increasing the piezoresistor's fractional resistance eventually increases sensor sensitivity with the longitudinal stresses applied in the *x*-, y-, and z-axis. W. Park *et al.* developed a tri-axial piezoresistive sensor integrated with a mechanical stopper to increase the stability and accuracy [97].

IV. High-frequency and Dual-frequency IVUS

IVUS imaging has been a gold standard for diagnosing coronary artery diseases for over two decades in both research and clinical practice. The IVUS instrument consists of a piezoelectric material lining along the catheter wire and a transducer. Electric current passes through the piezoelectric material to provide ultrasound by cycles of expansion and compression [98]. The transducer will receive the reflected ultrasound by the tissue, which will be converted to an ultrasound image. Depending on the type of tissue present (fibrous tissue, calcified tissue, lipid), the amount of ultrasound reflection will be different, creating contrast that can be seen in the image. Common working frequencies for IVUS are from 20 to 60 MHz. However, commercial IVUS transducers with 20 MHz to 40 MHz center frequencies are restricted with problems of reduced sensitivity, shortened penetration depth, and distorted beam profile [99]. Recently, Sung *et al.,* developed a high-frequency (>60 MHz) IVUS transducer by using asymmetric electrodes for improved beam profile [99, 100]. The new IVUS was built on asymmetric electrodes made from conductive and non-conductive backing blocks, which was verified by the analysis of the signal line of the extent of performance degradation. This system provided more uniform beam profile with better the signal to noise ratio in IVUS image.

IVUS and OCT two commonly used coronary artery imaging modalities. IVUS at 40-45 MHz has resolution on the order of 100 μm and penetration around 5~8 mm. On the other hand, OCT provides a much better resolution of 10-20 μm, but only 1.5 mm penetration depth is achievable. Our team researched on integrated IVUS-OCT catheters, which could provide high resolution for superficial micro-structures and moderate resolution for deep tissues [101, 102]. However, there is still a gap between conventional IVUS and OCT in resolution for tissues beyond the penetration depth of OCT. Obtaining high resolution is critical in quantifying and characterizing plaque burden. For example, the overlying thin-cap of the thin-cap fibroatheroma is usually less than 65 μm thick, which is less than the typical resolution for IVUS [103]. Increasing the center frequency to 80 MHz or higher can improve the imaging resolution and fill the gap between conventional IVUS and OCT, but at the cost of losing penetration depth. At 80 MHz, an attenuation

coefficient of 10 dB/mm is expected for the coronary artery, which means that a penetration depth of 3 mm can be achieved for a system with a dynamic range of 60 dB [104]. Although even higher frequency ultrasound transducers (100-300 MHz) are achievable, high attenuation in blood and poor penetration depth have limited their applications in IVUS [105].

Li *et al.* developed an 80 MHz intravascular ultrasound transducer made of PMN-PT free standing film, with a 65% bandwidth and 23 dB insertion loss [105]. Its aperture size is 0.4×0.4 mm^2. PMN-PT was chosen as the piezoelectric material due to high electrochemical coupling coefficient and superior dielectric constant. As shown in **Figure 4(a)-(c)**, the lateral and axial resolutions were measured as 176 μm and 35 μm [106]. Comparatively, commercial 40 MHz IVUS transducers normally have ~~a~~ lateral and axial resolutions around 60 μm and 300 μm. *In vitro* imaging of a normal rabbit aorta was performed to test the transducer's performance, as shown in **Figure 4(d)**. During the experiment, the tip of the transducer was positioned inside the lumen of the sample, which was immersed in water and supported by a sponge to stand in a water tank. For comparison, a 35 MHz transducer was fabricated with the same material and process, and it was tested with the same sample. **Figure 4(e)** shows the respective results for the 35 MHz transducer. Both were displayed with a 50-dB dynamic range. Results indicate that the 80 MHz transducer can better differentiate the endothelial wall and surrounding fatty tissue.

A later study from the same lab introduced transducers fabricated with PIN-PMN-PT. It was chosen for its electrical and thermal stability, which allows it to maintain higher bandwidth and sensitivity after the fabrication process compared to PMN-PT [107]. The higher electrochemical coupling coefficient and lower acoustic impedance leads to a better resolution even at a lower frequency. *Ex vivo* testing revealed that a 41 MHz PIN-PMN-PT transducer can image at a resolution of 43 μm.

As mentioned earlier, the major drawback in increasing the frequency of the IVUS transducer is the decrease in penetration depth due to high attenuation. A potential solution is the development of dual-frequency IVUS. Recently, Zhou's group developed a dual-frequency IVUS imaging system to integrate a conventional IVUS transducer (35 MHz) with an ultra-high frequency IVUS transducer (90-150 MHz) into

one single catheter. It was reported to successfully image a human coronary artery *in vitro* [108]. In this study, multiple frequency combinations were tested to determine the optimal balance between resolution and penetration depth. Considering the electrical impedance match, transducers with frequencies of 35 and 90 MHz were made of PMN-PT, while transducers with frequencies of 120 and 150 MHz were fabricated with LNO due to its lower dielectric permittivity and higher longitudinal sound speed [109]. The catheter adopted a back-to-back configuration, which not only allowed for a smaller catheter size but also provided easy co-registration. The overall size of the catheter is 0.95 mm in diameter with a front rigid length of 2 mm, which is comparable to the size of a commercial IVUS catheter and small enough to ensure the safety in potential clinical use.

Figure 5 shows the images of a human coronary artery that was imaged by multi-frequency catheters *in vitro*. **Figure 5(a)-(c)** are images of the same sample acquired by transducers in the respective frequencies of 35 MHz, 90 MHz and 120 MHz. These images were fused together to reveal more information of the artery as shown in **Figure 5(d)-(e)**. By combining the improved resolution from ultra-high frequency IVUS transducers and the deep imaging depth of conventional IVUS transducers, the *in vitro* human coronary artery imaging demonstrated the capability of the multi-frequency catheter to provide a more comprehensive visualization of the vascular structure and to facilitate the assessment of the vulnerable plaque. Looking at the data for the combinations of 35/90 MHz, 35/120 MHz, and 35/150 MHz, results indicate that the 35/90 MHz combination yielded the best resolution and penetration depth due to broader bandwidth. The 150 MHz transducer provided the worst results out of all high-frequency transducers tested due to shallow penetration depth and poor imaging contrast. Similar results were seen with a 36/78 MHz PMN-PT dual-frequency transducer, producing an axial resolution of 34 μm and a lateral resolution of 106 μm [110]. Compared with other multi-modality intravascular imaging techniques, this ultrasound-only imaging system was cost-effective and easy-to-use.

Dual-frequency intravascular transducers were also applied to harmonic imaging and acoustic angiography [110-112]. For instance, Jiang and Dayton's group reported a design and application of dual-

frequency IVUS transducers in intravascular super-harmonic contrast imaging and angiography [111]. The dual frequency transducer was designed as a stacked dual piezoelectric layer transduction structure. The high-frequency receiving transducer (37 MHz) was put on top of the low frequency excitation transducer (5.5 MHz). The two layers were acoustically isolated to prevent undesirable echoes and coupling using a frequency-selective isolation layer [113]. The ability of the system to detect micro-vessels was confirmed both *ex vivo* using porcine arteries and *in vivo* using the chorioallantoic membrane of a developing chicken embryo. The group also developed a dual-frequency (2.25/30 MHz) cylindrical array, which was applied to conduct real-time super-harmonic ultrasound angiography [114, 115]. Incorporating a PMN-PT transducer with 8 transmission elements and 32 receiving elements, the overall size was successfully controlled within 5 Fr (3 Fr = 1 mm) to fulfill the native size requirement for angiography. Compared to their single-element dual-frequency IVUS transducer, the array transducer provided a higher CNR (16.6 dB vs 11 dB), improved axial resolution (162 μm vs 616 μm), and real-time imaging speed.

Foster *et al.* have been working on dual-frequency IVUS imaging for over two decades [116, 117]. In their recent study, the design and fabrication of a 3-F dual-frequency catheter using a bidirectional PZT-5H transducer stack with center frequencies of approximately 30 and 80 MHz were described [117]. PZT was used because of its better stability over PMN-PT despite having less optimal technical specifications. The ability of the high-frequency transducer to achieve significantly improved axial and lateral resolution (16 and 120 μm, respectively, vs. 50 and 220 μm) at the expense of penetration depth was also discussed. A low-density polyethylene (LDPE) sheath was incorporated in the catheter to mimic the clinical situation. Noted issues include high insertion loss, rotational image distortion, and lowered sensitivity due to the sheath.

While these studies have shown improvements to the resolution of ultrasound images and better assessment to the morphological features of unstable plaques such as thin-cap fibroatheromas, *in vivo* testing needs to be done in the future to understand actual detection improvements and potential attenuation effects, as these studies have only verified through *in vitro* and/or *ex vivo* models. Blood was also indicated

to attenuate ultrasound, which leads to the drawback of flushing the transducer before measuring [118, 119].

V. Discussion and Conclusions

Studies have attempted to determine the association of plaque rupture to the physiological stenosis severity determined by fractional flow reserve and coronary flow reserve [120, 121]. The studies show abnormal region myocardial blood flow through the stress-induced distal perfusion pressure with FFR below 0.80, which results in hyperemia-induced vasodilation. Plaque rupture has been suggested to independently affect FFR values, but controversy exists regarding using FFR to determine plaque instability [87]. Recent reports have combined IVUS and FFR to study intermediate coronary lesions, in which results indicate that there were no differences in the amount of atheromatous plaque measured by those methods [87]. This could indicate that while FFR is currently the optimal measurement for plaque instability, it needs to be combined with other methods for standardization or optimization. Future studies should be conducted to determine the possible relationship between plaque morphology and FFR (and possibly additional modalities, such as optical coherence tomography, or OCT). Studies have suggested that other diagnostic tools, such as CCTA and electrical impedance spectroscopy (EIS), should be used in tandem with FFR to provide a more accurate diagnosis.

In recent studies, CCTA is combined with FFR for the detection of lesion-specific ischemia in order to improve coronary stenoses measurement noninvasively [122, 123]. Measuring fractional flow reserve by CCTA (FFR_{CT}) has also been proved to be a feasible and safe alternative to the conventional invasive fractional flow reserve measurement [124]. Some researchers proposed techniques to improve the accuracy and reliability of noninvasive FFR or FFR_{CT} [125, 126]. In 2018, Dey D *et al*. used integrated machine learning for calculating the ischemia risk score to predict lesion-specific ischemia [67]. This provides better outcomes compared with quantitative plaque measures. Studies show that while CCTA and FFR_{CT} display equivalent clinical outcomes and quality of life, CCTA induces lower costs.

Electrochemical impedance spectroscopy (EIS) is an approach to measure frequency-related impedance of an electrochemical system, which can reveal the underlying electrochemical properties of unstable plaques. Plaques display distinct electrochemical properties, which provides differentiation between various grades of plaques [127]. Our team reported increases in frequency-dependent electrochemical impedance magnitude in explants of atherosclerotic lesions in the human aortic arch by nearly 1.5-fold compared to lesion-free sites [128]. Since blood vessels harbor resistance and store charges, complex electric impedance (Z) as a function of frequency is exhibited on vessels. An alternating voltage is applied to the site of interest, and the frequency dependent electric impedance can be calculated with the measured current. Using equivalent circuits to simulate the impedance changes in magnitude and in phase across a sweeping-frequency range, the underlying electrochemical properties can be revealed.

To obtain the EIS measurement of a plaque site, a typical EIS sensor contains 2 electrodes that contact tissue. The impedance between the electrodes is considered as the tissue impedance. Some of the sensors utilize the inflatable balloon structure to increase the pressure and contact area to obtain more accurate results. We developed an EIS sensor to detect lipid-rich lesions in New Zealand white rabbits [49]. The concentric bipolar micro sensor is glued on the surface of a micro balloon. We also conducted EIS measurements with a catheter-based 2-point micro-electrode and validations with IVUS system [51]. We then further developed an IVUS-guided EIS sensor to decrease variability and increase reproducibility in measurement and detection [129]. The integrated configuration is shown in **Figure 6**. The IVUS transducer allows better alignment between the EIS sensor and the lesion. Because of the safety and relatively simple deployment of an invasive EIS sensor, it is valuable for further development of EIS technique. Furthermore, in order to acquire more complete and accurate results, EIS sensors can be integrated with IVUS and other techniques.

The vulnerable plaque is a major cause of acute cardiovascular conditions, such as myocardial infarction. Because of the plaque's propensity to rupture, it can lead to repeated incidents of stenosis in blood vessels. Therefore, identifying vulnerable plaques is critical to providing the most appropriate

treatment for the patient. While coronary angiography is the gold standard for imaging the whole coronary vessel system, it fails to distinguish vulnerable plaques due to the lack of spatial and temporal resolution or deficient information in structural composition. Recent research has explored various imaging modalities and sensors to identify vulnerable plaques based on the specific qualities of the plaque. Each modality has its own strengths and weaknesses, leading researchers to develop combinatorial strategies for utilizing multiple functionalities while reducing limitations. For example, PET-CT imaging with ^{18}F-NaF ultilizes the overall structural imaging from CT-scanning and the identification of calcified regions seen in vulnerable plaques in the coronary arteries from PET with the sodium fluoride tracer. However, limitations such as the difficulty in localizing the tracer and potential artifacts such as cardiac and respiratory motion can decrease the effectiveness of the modality. Fractional flow reserve is an accurate and simple way to assess the functional significance of plaques in the coronary artery. MEMS technology is widely utilized to fabricate nanoscale and low-cost pressure sensors to assist obtaining pressure *in vivo*. To provide better visualization of the thin fibrous cap seen in vulnerable plaques, high-frequency IVUS is developed to increase the spatial resolution. Unfortunately, this has resulted in the decrease in penetration depth in imaging. A potential solution is the incorporation of both low-frequency and high-frequency transducers in dual-frequency IVUS for suitable spatial resolution and penetration depth. While studies have demonstrated the feasibility of high/dual-frequency IVUS, *in vivo* testing has not been done to verify the capability of these modalities to identify vulnerable plaques.

Acknowledgements

This work is supported by the National Science Foundation CAREER Award #1652818 under Hung Cao.

Figures and captions

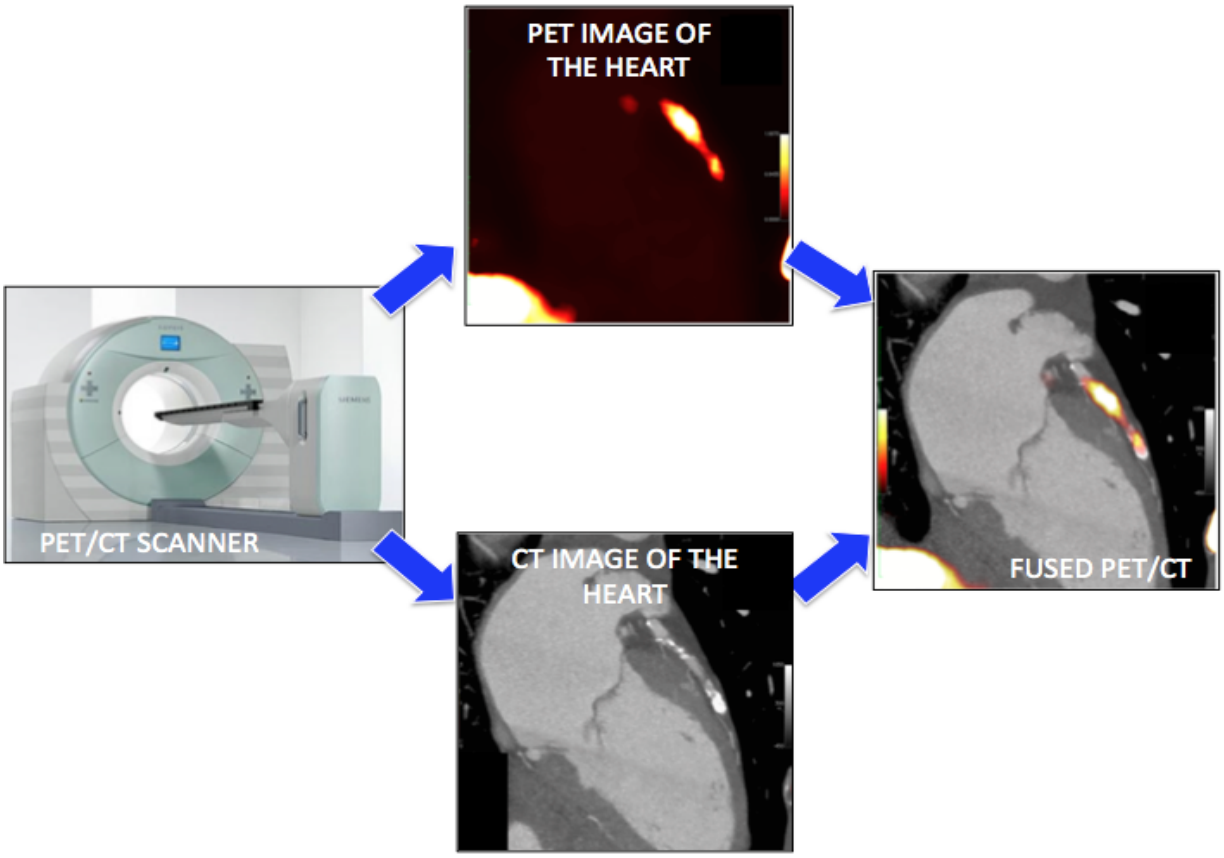

Figure 1. How 18F-NaF PET-CT works. PET-CT scanners combine information about biological activity (in this case microcalcification using ^{18}F-Fluoride) from the PET scanner with anatomical information of the heart from CT. When these images are fused together the microcalcification activity can be localized to a specific plaque within the coronary arteries.

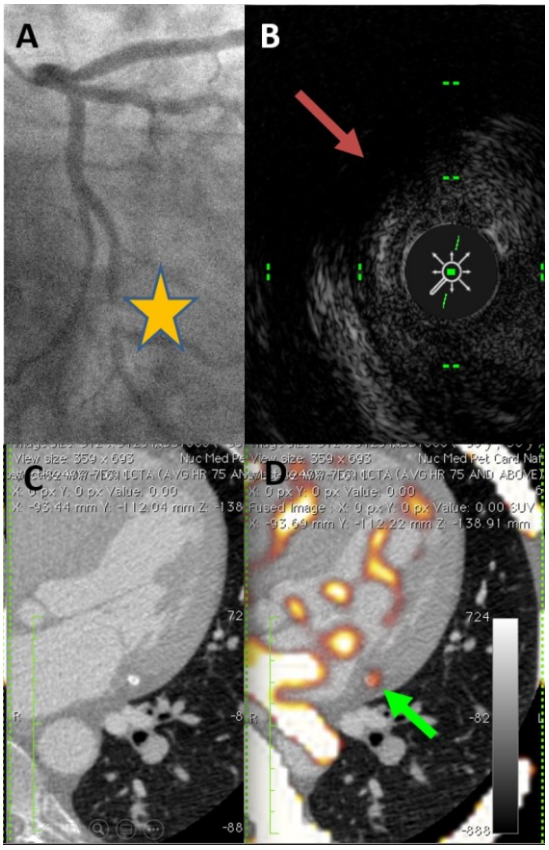

Figure 2. Panel of images demonstrate a ^{18}F-NaF acquired at Cedars-Sinai Heart Institute. Panel A shows the patient's distal circumflex lesion (yellow star) with corresponding 60 MHz IVUS image (Panel B) showing lipid-rich plaque with ultrasound attenuation from 9 to 12 o'clock (red arrow). Panels C and D show a non-fused and fused CCTA, respectively. Panel D shows NaF uptake in the distal portion of the left circumflex corresponding to the patient's area of acute infarction and presentation with acute coronary syndrome (green arrow).

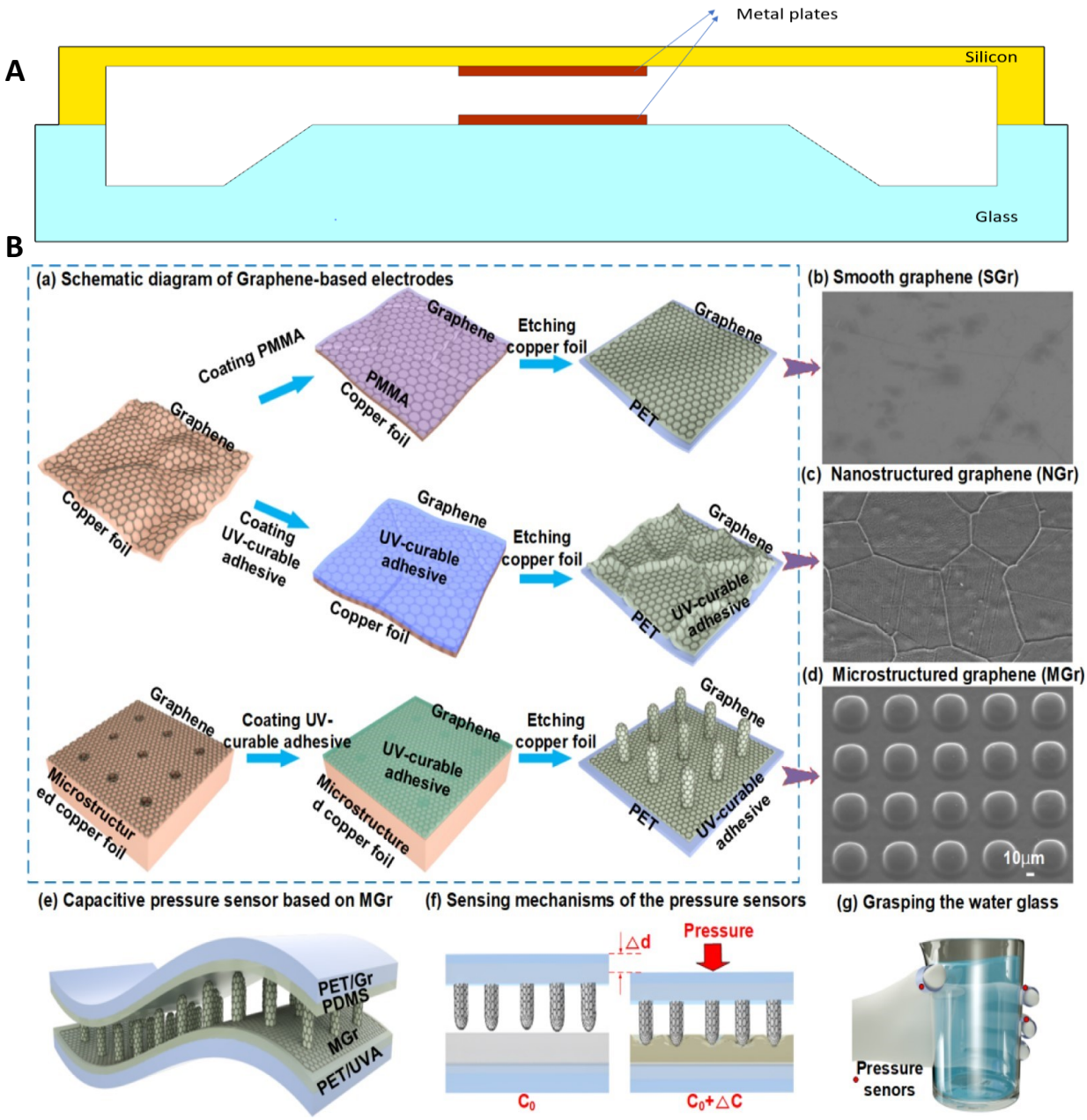

Figure 3. (A) Cross section of a simple capacitive pressure sensor. (B) Fabrication of the flexible pressure sensors based on microconformal graphene electrodes. (B-a) Illustration diagram of fabrication process for different conformal graphene electrodes. (B(b−d)) SEM images of smooth graphene electrodes (SGrE), nanostructured graphene electrode (NGrE), and microstructured graphene electrode (MGrE) derived from PMMA-based, UVA-based and microconformal transfer methods, respectively. (B(e)) Illustration ofcapacitive pressure sensor based on MGrE. (B(f)) Schematic diagram of sensing mechanisms. (B(g)) Schematic diagram of grasping with the proposed pressure sensor [91].

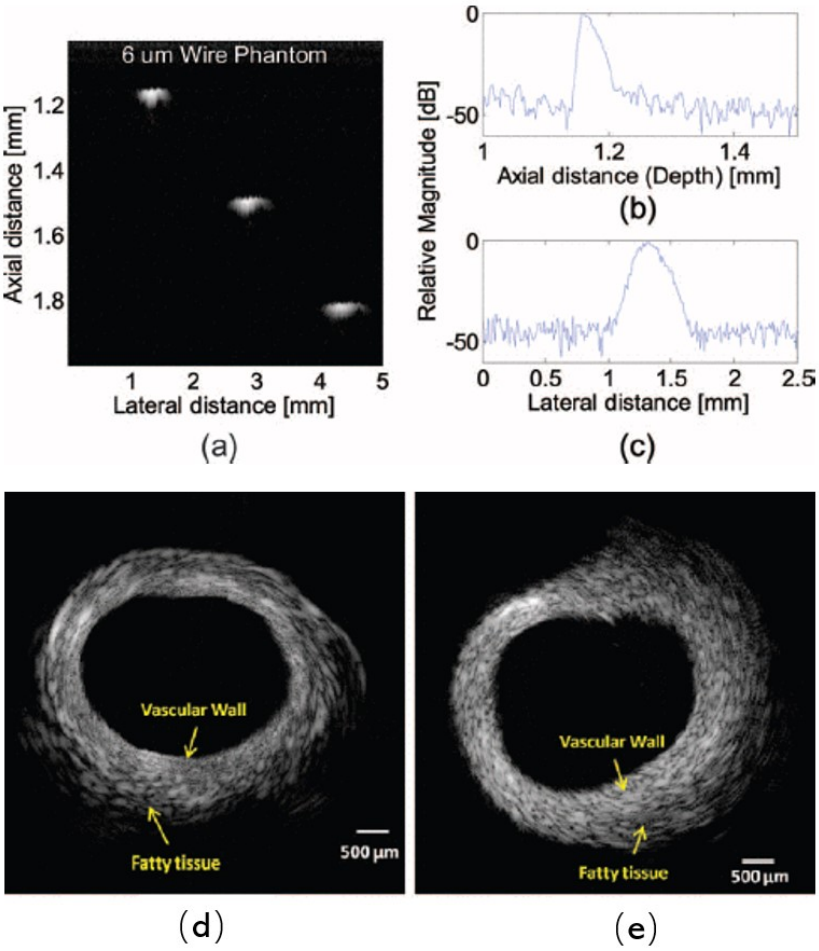

Figure 4. (a) Ultrasound wire phantom, displayed with a dynamic range of 45 dB; (b) axial and (c) lateral envelopes of echo signals from the wire located 1.2 mm away from the transducer surface. (d) Images of healthy rabbit aorta from 80-mHz PMN-PT free-standing-film transducer; and (e) 35-mHz PMN-PT single-crystal transducer.

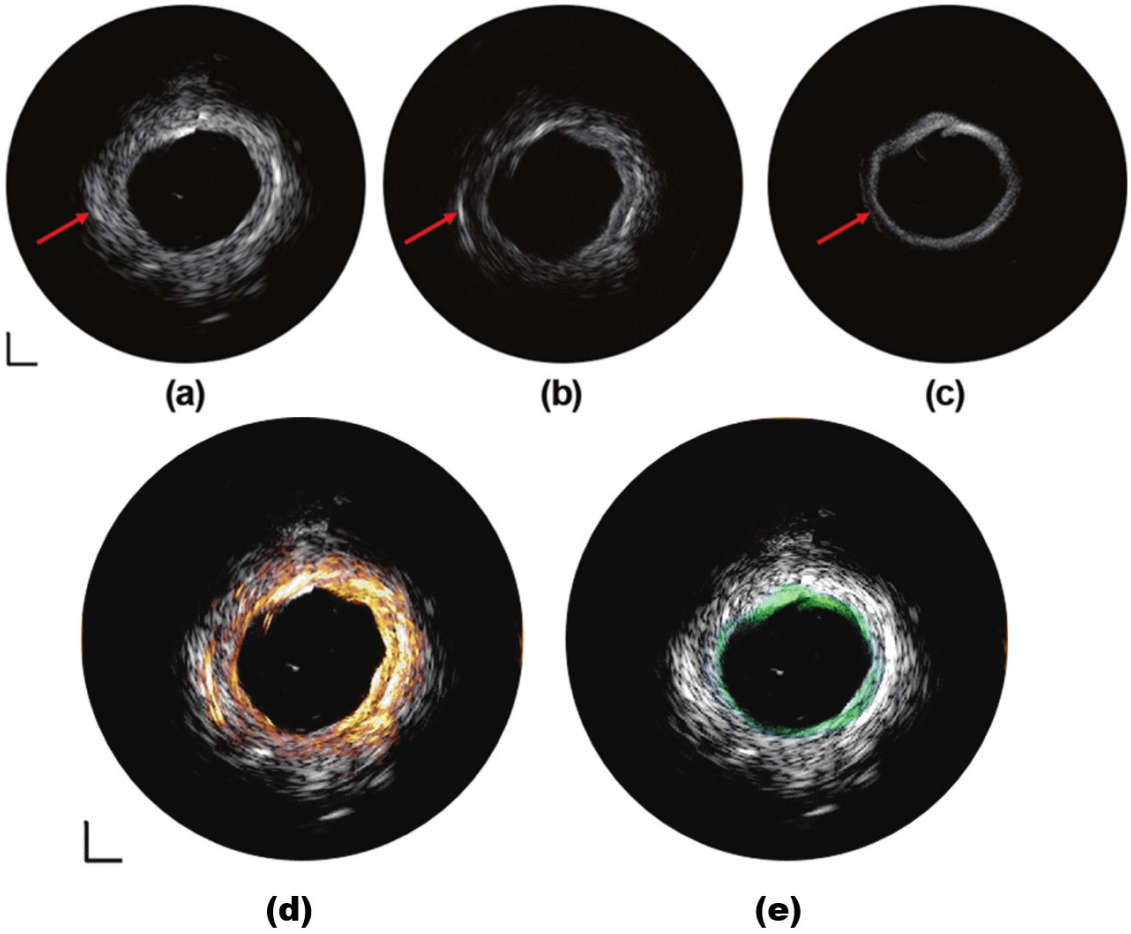

Figure 5. IVUS images of human coronary artery at (a) 35 MHz, (b) 90 MHz, and (c) 120 MHz. Fused IVUS images of human coronary artery captured by (d) 35/90-MHz multi-frequency IVUS catheter and (e) 35/120-MHz multifrequency IVUS catheter. White: 35-MHz IVUS image. Orange: 90-MHz IVUS image. Green: 120-MHz IVUS image. dynamic range: 50 dB. Scale bar: 1 mm.

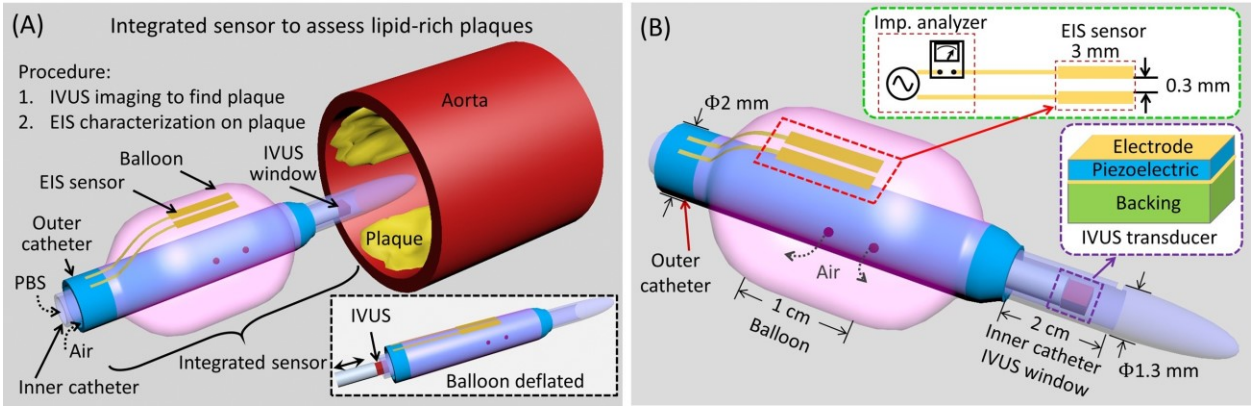

Figure 6. (A) Schematic of the IVUS-guided EIS sensor for better detection of unstable plaques in the artery. The IVUS transducer determines the positioning of the catheter and EIS sensor in relation to the plaque, providing optimal measurement for the EIS sensor. (B) More-detailed schematic for the EIS sensor. Attachment of the EIS sensor to the balloon allows radial adjustment from 2.3 mm to 6 mm in diameter by inflating or deflating the balloon by air. The EIS sensor consists of a 2-point electrode configuration, with each electrode 3 mm in length, 0.3 mm in width, and spaced 0.3 mm apart [129].

References

[1] N. R. Madamanchi, A. Vendrov, and M. S. Runge, "Oxidative stress and vascular disease," *Arterioscl. Throm. Vas.,* vol. 25, pp. 29-38, 2005.

[2] P. F. Davies, A. Remuzzi, E. J. Gordon, C. F. Dewey, and M. A. Gimbrone, "Turbulent fluid shear stress induces vascular endothelial cell turnover in vitro," *P. Natl. Acad. Sci.,* vol. 83, pp. 2114-2117, 1986.

[3] J. Bamford, P. Sandercock, M. Dennis, C. Warlow, and J. Burn, "Classification and natural history of clinically identifiable subtypes of cerebral infarction," *The Lancet,* vol. 337, pp. 1521-1526, 1991.

[4] R. Virmani, A. P. BURKE, F. D. KOLODGIE, and A. Farb, "Vulnerable plaque: the pathology of unstable coronary lesions," *J. Interv. Cardiol.,* vol. 15, pp. 439-446, 2002.

[5] R. Virmani, A. P. Burke, A. Farb, and F. D. Kolodgie, "Pathology of the unstable plaque," *Prog. Cardiovasc. Dis.,* vol. 44, pp. 349-356, 2002.

[6] B. D. MacNeill, H. C. Lowe, M. Takano, V. Fuster, and I.-K. Jang, "Intravascular modalities for detection of vulnerable plaque current status," *Arteriosclerosis, thrombosis, and vascular biology,* vol. 23, pp. 1333-1342, 2003.

[7] G. A. Roth, C. Johnson, A. Abajobir, F. Abd-Allah, S. F. Abera, G. Abyu*, et al.*, "Global, Regional, and National Burden of Cardiovascular Diseases for 10 Causes, 1990 to 2015," *Journal of the American College of Cardiology,* vol. 70, pp. 1-25, 2017.

[8] P. D. Richardson, M. Davies, and G. Born, "Influence of plaque configuration and stress distribution on fissuring of coronary atherosclerotic plaques," *The Lancet,* vol. 334, pp. 941-944, 1989.

[9] R. Virmani, F. D. Kolodgie, A. P. Burke, A. Farb, and S. M. Schwartz, "Lessons from sudden coronary death a comprehensive morphological classification scheme for atherosclerotic lesions," *Arteriosclerosis, thrombosis, and vascular biology,* vol. 20, pp. 1262-1275, 2000.

[10] J. A. Schaar, J. E. Muller, E. Falk, R. Virmani, V. Fuster, P. W. Serruys*, et al.*, "Terminology for high-risk and vulnerable coronary artery plaques," *European heart journal,* vol. 25, pp. 1077-1082, 2004.

[11] K. Jansen, G. van Soest, and A. F. van der Steen, "Intravascular photoacoustic imaging: a new tool for vulnerable plaque identification," *Ultrasound in medicine & biology,* vol. 40, pp. 1037-1048, 2014.

[12] G. W. Stone, A. Maehara, A. J. Lansky, B. de Bruyne, E. Cristea, G. S. Mintz*, et al.*, "A prospective natural-history study of coronary atherosclerosis," *New England Journal of Medicine,* vol. 364, pp. 226-235, 2011.

[13] N. W. Shammas, "Epidemiology, classification, and modifiable risk factors of peripheral arterial disease," *Vascular Health and Risk Management,* vol. 3, pp. 229-234, 2007.

[14] D. Rizik and J. A. Goldstein, "NIRS-IVUS imaging to characterize the composition and structure of coronary plaques," ed: HMP COMMUNICATIONS 83 GENERAL WARREN BLVD, STE 100, MALVERN, PA 19355 USA, 2013.

[15] F. Kolodgie, R. Virmani, A. Burke, A. Farb, D. Weber, R. Kutys*, et al.*, "Pathologic assessment of the vulnerable human coronary plaque," *Heart,* vol. 90, pp. 1385-1391, 2004.

[16] Y. Ding, P. A. Long, J. M. Bos, Y. H. Shih, X. Ma, R. S. Sundsbak*, et al.*, "A modifier screen identifies DNAJB6 as a cardiomyopathy susceptibility gene," *JCI Insight* vol. 1(14):e88797. doi:10.1172/jci.insight.88797. , 2016.

[17] D. Yeager, Y.-S. Chen, S. Litovsky, and S. Emelianov, "Intravascular photoacoustics for image-guidance and temperature monitoring during plasmonic photothermal therapy of atherosclerotic plaques: a feasibility study," *Theranostics,* vol. 4, p. 36, 2014.

[18] N. R. Mollet, F. Cademartiri, C. A. van Mieghem, G. Runza, E. P. McFadden, T. Baks*, et al.*, "High-resolution spiral computed tomography coronary angiography in patients referred for diagnostic conventional coronary angiography," *Circulation,* vol. 112, pp. 2318-2323, 2005.
[19] S. Achenbach, "Computed tomography coronary angiography," *Journal of the American College of Cardiology,* vol. 48, pp. 1919-1928, 2006.
[20] G. L. Raff, M. J. Gallagher, W. W. O'Neill, and J. A. Goldstein, "Diagnostic accuracy of noninvasive coronary angiography using 64-slice spiral computed tomography," *Journal of the American College of Cardiology,* vol. 46, pp. 552-557, 2005.
[21] Z. A. Fayad, V. Fuster, J. T. Fallon, T. Jayasundera, S. G. Worthley, G. Helft*, et al.*, "Noninvasive in vivo human coronary artery lumen and wall imaging using black-blood magnetic resonance imaging," *Circulation,* vol. 102, pp. 506-510, 2000.
[22] T. S. Hatsukami, R. Ross, N. L. Polissar, and C. Yuan, "Visualization of fibrous cap thickness and rupture in human atherosclerotic carotid plaque in vivo with high-resolution magnetic resonance imaging," *Circulation,* vol. 102, pp. 959-964, 2000.
[23] S. G. Ruehm, C. Corot, P. Vogt, S. Kolb, and J. F. Debatin, "Magnetic resonance imaging of atherosclerotic plaque with ultrasmall superparamagnetic particles of iron oxide in hyperlipidemic rabbits," *Circulation,* vol. 103, pp. 415-422, 2001.
[24] T. Ueda, S. Sakaki, W. T. Yuh, I. Nochide, and S. Ohta, "Outcome in acute stroke with successful intra-arterial thrombolysis and predictive value of initial single-photon emission-computed tomography," *Journal of Cerebral Blood Flow & Metabolism,* vol. 19, pp. 99-108, 1999.
[25] S. A. Chamuleau, M. Meuwissen, B. L. van Eck-Smit, K. T. Koch, A. de Jong, R. J. de Winter*, et al.*, "Fractional flow reserve, absolute and relative coronary blood flow velocity reserve in relation to the results of technetium-99m sestambi single-photon emission computed tomography in patients with two-vessel coronary artery disease," *Journal of the American College of Cardiology,* vol. 37, pp. 1316-1322, 2001.
[26] E.-K. Choi, E. J. Chun, S.-I. Choi, S.-A. Chang, S.-H. Choi, S. Lim*, et al.*, "Assessment of subclinical coronary atherosclerosis in asymptomatic patients with type 2 diabetes mellitus with single photon emission computed tomography and coronary computed tomography angiography," *The American journal of cardiology,* vol. 104, pp. 890-896, 2009.
[27] A. Tawakol, R. Q. Migrino, U. Hoffmann, S. Abbara, S. Houser, H. Gewirtz*, et al.*, "Noninvasive in vivo measurement of vascular inflammation with F-18 fluorodeoxyglucose positron emission tomography," *Journal of nuclear cardiology,* vol. 12, pp. 294-301, 2005.
[28] J. H. Rudd, J. Narula, H. W. Strauss, R. Virmani, J. Machac, M. Klimas*, et al.*, "Imaging atherosclerotic plaque inflammation by fluorodeoxyglucose with positron emission tomography: ready for prime time?," *Journal of the American College of Cardiology,* vol. 55, pp. 2527-2535, 2010.
[29] A. L. Figueroa, S. S. Subramanian, R. C. Cury, Q. A. Truong, J. A. Gardecki, G. J. Tearney*, et al.*, "Distribution of inflammation within carotid atherosclerotic plaques with high-risk morphological features a comparison between positron emission tomography activity, plaque morphology, and histopathology," *Circulation: Cardiovascular Imaging,* vol. 5, pp. 69-77, 2012.
[30] T. Ma, B. Zhou, T. K. Hsiai, and K. K. Shung, "A Review of Intravascular Ultrasound–Based Multimodal Intravascular Imaging The Synergistic Approach to Characterizing Vulnerable Plaques," *Ultrasonic Imaging,* p. 0161734615604829, 2015.
[31] D.-H. Kim, N. Lu, R. Ma, Y.-S. Kim, R.-H. Kim, S. Wang*, et al.*, "Epidermal electronics," *Science,* vol. 333, pp. 838-843, 2011.
[32] H. Cao, V. Landge, U. Tata, Y.-S. Seo, S. Rao, S.-J. Tang*, et al.*, "An implantable, batteryless, and wireless capsule with integrated impedance and pH sensors for gastroesophageal reflux monitoring," *Biomedical Engineering, IEEE Transactions on,* vol. 59, pp. 3131-3139, 2012.
[33] M. Caldorera-Moore and N. A. Peppas, "Micro-and nanotechnologies for intelligent and responsive biomaterial-based medical systems," *Advanced drug delivery reviews,* vol. 61, pp. 1391-1401, 2009.

[34] H. Cao, A.-L. Li, C. M. Nguyen, Y.-B. Peng, and J.-C. Chiao, "An integrated flexible implantable micro-probe for sensing neurotransmitters," *Sensors Journal, IEEE,* vol. 12, pp. 1618-1624, 2012.
[35] C. M. Gardner, H. Tan, E. L. Hull, J. B. Lisauskas, S. T. Sum, T. M. Meese*, et al.*, "Detection of lipid core coronary plaques in autopsy specimens with a novel catheter-based near-infrared spectroscopy system," *JACC: Cardiovascular Imaging,* vol. 1, pp. 638-648, 2008.
[36] S. Garg, P. W. Serruys, M. van der Ent, C. Schultz, F. Mastik, G. van Soest*, et al.*, "First use in patients of a combined near infra-red spectroscopy and intra-vascular ultrasound catheter to identify composition and structure of coronary plaque," *EuroIntervention: journal of EuroPCR in collaboration with the Working Group on Interventional Cardiology of the European Society of Cardiology,* vol. 5, p. 755, 2010.
[37] P. R. Moreno, R. A. Lodder, K. R. Purushothaman, W. E. Charash, W. N. O'Connor, and J. E. Muller, "Detection of lipid pool, thin fibrous cap, and inflammatory cells in human aortic atherosclerotic plaques by near-infrared spectroscopy," *Circulation,* vol. 105, pp. 923-927, 2002.
[38] X. Bai, X. Gong, R. Lin, W. Hau, and L. Song, "Integrated intravascular ultrasound and optical-resolution photoacoustic microscopy with a 1-mm-diameter catheter," in *SPIE BiOS*, 2014, pp. 894308-894308-7.
[39] R. N. MacAlpin, A. S. Abbasi, J. H. Grollman, and L. Eber, "Human Coronary Artery Size During Life," *Radiology,* vol. 108, pp. 567-576, 1973/09/01 1973.
[40] A. N. Kharlamov and J. L. Gabinsky, "Plasmonic photothermic and stem cell therapy of atherosclerotic plaque as a novel nanotool for angioplasty and artery remodeling," *Rejuvenation research,* vol. 15, pp. 222-230, 2012.
[41] A. Kharlamov, A. Tyurnina, V. Veselova, O. Novoselova, A. Filatova, and O. Kovtun, "Plasmonics for treatment of atherosclerosis: results of NANOM-FIM trial," *J Nanomed Nanotechol,* vol. 4, p. 2, 2013.
[42] C. Baer, G. Notzon, C. Dahl, C. Schulz, B. Will, I. Rolfes*, et al.*, "A millimeter-wave based measuring method for the differentiation of atherosclerotic plaques," in *Microwave Workshop Series on RF and Wireless Technologies for Biomedical and Healthcare Applications (IMWS-BIO), 2013 IEEE MTT-S International*, 2013, pp. 1-4.
[43] G. Notzon, C. Baer, T. Musch, C. Dahl, and I. Rolfes, "Conformal mm-wave antennas for catheter embedded atherosclerotic plaque sensors," in *2015 European Microwave Conference (EuMC)*, 2015, pp. 825-828.
[44] M. Rouhanizadeh, T. Tang, C. Li, G. Soundararajan, C. Zhou, and T. Hsiai, "Applying indium oxide nanowires as sensitive and selective redox protein sensors," in *2004. 17th IEEE Intl. Conf. MEMS*, 2004, pp. 434-437.
[45] J. Hwang, M. Rouhanizadeh, R. T. Hamilton, T. C. Lin, J. P. Eiserich, H. N. Hodis*, et al.*, "17β-Estradiol reverses shear-stress-mediated low density lipoprotein modifications," *Free Radical Bio. Med.,* vol. 41, pp. 568-578, 2006.
[46] F. Yu, X. Dai, T. Beebe, and T. K. Hsiai, "Electrochemical impedance spectroscopy to characterize inflammatory atherosclerotic plaques," *Biosens. Bioelectron.,* vol. 30, pp. 165-173, 2011.
[47] L. Ai, M. Rouhanizadeh, J. C. Wu, W. Takabe, H. Yu, M. Alavi*, et al.*, "Shear stress influences spatial variations in vascular Mn-SOD expression: implication for LDL nitration," *Am. J. Physiol.-Cell Ph.,* vol. 294, pp. C1576-C1585, 2008.
[48] F. Yu, R. Li, L. Ai, C. Edington, H. Yu, M. Barr*, et al.*, "Electrochemical Impedance Spectroscopy to Assess Vascular Oxidative Stress," *Ann. Biomed. Eng.,* vol. 39, pp. 287-296, 2011.
[49] H. Cao, F. Yu, Y. Zhao, N. Scianmarello, J. Lee, W. Dai*, et al.*, "Stretchable electrochemical impedance sensors for intravascular detection of lipid-rich lesions in New Zealand White rabbits," *Biosens. Bioelectron.,* vol. 54, pp. 610-616, 2014.

[50] R. R. S. Packard, Y. Luo, P. Abiri, N. Jen, O. Aksoy, W. M. Suh*, et al.*, "3-D Electrochemical Impedance Spectroscopy Mapping of Arteries to Detect Metabolically Active but Angiographically Invisible Atherosclerotic Lesions," *Theranostics,* vol. 7, pp. 2431-2442, 2017.
[51] R. R. S. Packard, X. Zhang, Y. Luo, T. Ma, N. Jen, J. Ma*, et al.*, "Two-Point Stretchable Electrode Array for Endoluminal Electrochemical Impedance Spectroscopy Measurements of Lipid-Laden Atherosclerotic Plaques," *Annals of biomedical engineering,* pp. 1-12, 2016.
[52] F. Leuschner and M. Nahrendorf, "Molecular imaging of coronary atherosclerosis and myocardial infarction: considerations for the bench and perspectives for the clinic," *Circ Res,* vol. 108, pp. 593-606, Mar 4 2011.
[53] A. Irkle, A. T. Vesey, D. Y. Lewis, J. N. Skepper, J. L. E. Bird, M. R. Dweck*, et al.*, "Identifying active vascular microcalcification by 18F-sodium fluoride positron emission tomography," *Nature Communications,* vol. 6, p. 7495, 2015/07/07 2015.
[54] J. D. Hutcheson, N. Maldonado, and E. Aikawa, "Small entities with large impact: microcalcifications and atherosclerotic plaque vulnerability," *Curr Opin Lipidol,* vol. 25, pp. 327-32, Oct 2014.
[55] E. Balogh, A. Tóth, G. Méhes, G. Trencsényi, G. Paragh, and V. Jeney, "Hypoxia Triggers Osteochondrogenic Differentiation of Vascular Smooth Muscle Cells in an HIF-1 (Hypoxia-Inducible Factor 1)–Dependent and Reactive Oxygen Species–Dependent Manner," *Arteriosclerosis, Thrombosis, and Vascular Biology,* vol. 39, pp. 1088-1099, 2019.
[56] L. L. Demer and Y. Tintut, "Vascular Calcification," *Circulation,* vol. 117, pp. 2938-2948, 2008.
[57] K. Benz, K.-F. Hilgers, C. Daniel, and K. Amann, "Vascular Calcification in Chronic Kidney Disease: The Role of Inflammation," *International journal of nephrology,* vol. 2018, pp. 4310379-4310379, 2018.
[58] L. L. Demer and Y. Tintut, "Inflammatory, metabolic, and genetic mechanisms of vascular calcification," *Arterioscler Thromb Vasc Biol,* vol. 34, pp. 715-23, Apr 2014.
[59] A. Irkle, A. T. Vesey, D. Y. Lewis, J. N. Skepper, J. L. Bird, M. R. Dweck*, et al.*, "Identifying active vascular microcalcification by (18)F-sodium fluoride positron emission tomography," *Nat Commun,* vol. 6, p. 7495, 2015.
[60] E. Aikawa, M. Nahrendorf, J.-L. Figueiredo, F. K. Swirski, T. Shtatland, R. H. Kohler*, et al.*, "Osteogenesis Associates With Inflammation in Early-Stage Atherosclerosis Evaluated by Molecular Imaging In Vivo," *Circulation,* vol. 116, pp. 2841-2850, 2007.
[61] A. Kelly-Arnold, N. Maldonado, D. Laudier, E. Aikawa, L. Cardoso, and S. Weinbaum, "Revised microcalcification hypothesis for fibrous cap rupture in human coronary arteries," *Proc Natl Acad Sci U S A,* vol. 110, pp. 10741-6, Jun 25 2013.
[62] N. V. Joshi, A. T. Vesey, M. C. Williams, A. S. Shah, P. A. Calvert, F. H. Craighead*, et al.*, "18F-fluoride positron emission tomography for identification of ruptured and high-risk coronary atherosclerotic plaques: a prospective clinical trial," *Lancet,* vol. 383, pp. 705-13, Feb 22 2014.
[63] M. Rubeaux, N. V. Joshi, M. R. Dweck, A. Fletcher, M. Motwani, L. E. Thomson*, et al.*, "Motion Correction of 18F-NaF PET for Imaging Coronary Atherosclerotic Plaques," *J Nucl Med,* vol. 57, pp. 54-9, Jan 2016.
[64] S. Gaur, K. A. Øvrehus, D. Dey, J. Leipsic, H. E. Bøtker, J. M. Jensen*, et al.*, "Coronary plaque quantification and fractional flow reserve by coronary computed tomography angiography identify ischaemia-causing lesions," *European heart journal,* vol. 37, pp. 1220-1227, 2016.
[65] V. E. Stegehuis, G. W. Wijntjens, J. J. Piek, and T. P. van de Hoef, "Fractional Flow Reserve or Coronary Flow Reserve for the Assessment of Myocardial Perfusion : Implications of FFR as an Imperfect Reference Standard for Myocardial Ischemia," *Current cardiology reports,* vol. 20, pp. 77-77, 2018.
[66] S. Vijayan, D. S. Barmby, I. R. Pearson, A. G. Davies, S. B. Wheatcroft, and M. Sivananthan, "Assessing Coronary Blood Flow Physiology in the Cardiac Catheterisation Laboratory," *Current cardiology reviews,* vol. 13, pp. 232-243, 2017.

[67] D. Dey, S. Gaur, K. A. Ovrehus, P. J. Slomka, J. Betancur, M. Goeller, *et al.*, "Integrated prediction of lesion-specific ischaemia from quantitative coronary CT angiography using machine learning: a multicentre study," *European Radiology,* vol. 28, pp. 2655-2664, 2018/06/01 2018.
[68] D. Corcoran, B. Hennigan, and C. Berry, "Fractional flow reserve: a clinical perspective," *The international journal of cardiovascular imaging,* vol. 33, pp. 961-974, 2017.
[69] N. V. Pothineni, N. N. Shah, Y. Rochlani, R. Nairooz, S. Raina, M. A. Leesar, *et al.*, "U.S. Trends in Inpatient Utilization of Fractional Flow Reserve and Percutaneous Coronary Intervention," *Journal of the American College of Cardiology,* vol. 67, pp. 732-733, 2016/02/16/ 2016.
[70] A. H. Seto, D. Tehrani, and M. J. Kern, "Limitations and Pitfalls of Fractional Flow Reserve Measurements and Adenosine-Induced Hyperemia," *Interventional Cardiology Clinics,* vol. 4, pp. 419-434, 2015/10/01/ 2015.
[71] N. Xue, C. Wang, C. X. Liu, and J. H. Sun, "Highly Integrated MEMS-ASIC Sensing System for Intracorporeal Physiological Condition Monitoring," *Sensors,* vol. 18, Jan 2018.
[72] B. E. Stahli, A. Erbay, J. Steiner, J. Klotsche, H. C. Mochmann, C. Skurk, *et al.*, "Comparison of resting distal to aortic coronary pressure with angiography-based quantitative flow ratio," *International Journal of Cardiology,* vol. 279, pp. 12-17, Mar 2019.
[73] J. Torrado, L. Buckley, A. Durán, P. Trujillo, S. Toldo, J. Valle Raleigh, *et al.*, "Restenosis, Stent Thrombosis, and Bleeding Complications," *Journal of the American College of Cardiology,* vol. 71, p. 1676, 2018.
[74] C. Berry, D. Corcoran, B. Hennigan, S. Watkins, J. Layland, and K. G. Oldroyd, "Fractional flow reserve-guided management in stable coronary disease and acute myocardial infarction: recent developments," *European heart journal,* vol. 36, pp. 3155-3164, 2015.
[75] G. Niccoli, C. Indolfi, and J. E. Davies, "Evaluation of intermediate coronary stenoses in acute coronary syndromes using pressure guidewire," *Open heart,* vol. 4, pp. e000431-e000431, 2017.
[76] S. Takarada, Z. Zhang, and S. Molloi, "An angiographic technique for coronary fractional flow reserve measurement: in vivo validation," *The international journal of cardiovascular imaging,* vol. 29, pp. 535-544, 2013.
[77] R. J. McGeoch and K. G. Oldroyd, "Pharmacological options for inducing maximal hyperaemia during studies of coronary physiology," *Catheterization and Cardiovascular Interventions,* vol. 71, pp. 198-204, 2008/02/01 2008.
[78] A. Mehra and B. Mohan, "Value of FFR in clinical practice," *Indian heart journal,* vol. 67, pp. 77-80, Jan-Feb 2015.
[79] R. Nakanishi and M. J. Budoff, "Noninvasive FFR derived from coronary CT angiography in the management of coronary artery disease: technology and clinical update," *Vascular health and risk management,* vol. 12, pp. 269-278, 2016.
[80] H. Arora, W. Posligua, and A. Mesa, "Use of fractional flow reserve and intravascular ultrasonography to evaluate ambiguous left main coronary artery stenosis," *Texas Heart Institute journal,* vol. 35, pp. 329-333, 2008.
[81] R. Ramadan, W. E. Boden, and S. Kinlay, "Management of Left Main Coronary Artery Disease," *Journal of the American Heart Association,* vol. 7, p. e008151, 2018.
[82] R. Petraco, S. Sen, S. Nijjer, M. Echavarria-Pinto, J. Escaned, D. P. Francis, *et al.*, "Fractional Flow Reserve–Guided Revascularization: Practical Implications of a Diagnostic Gray Zone and Measurement Variability on Clinical Decisions," *JACC: Cardiovascular Interventions,* vol. 6, pp. 222-225, 2013/03/01/ 2013.
[83] A. Jeremias, A. J. Kirtane, and G. W. Stone, "A Test in Context: Fractional Flow Reserve: Accuracy, Prognostic Implications, and Limitations," *Journal of the American College of Cardiology,* vol. 69, pp. 2748-2758, 2017/06/06/ 2017.
[84] A. Kärkkäinen, J. Saarilahti, J. Kyynäräinen, and H. Kuisma, "New MEMS Pressure Sensor Element and Concept for Coronary Catheter," *Procedia Engineering,* vol. 168, pp. 76-79, 2016/01/01/ 2016.

[85] I. Pantos and D. Katritsis, "Fractional Flow Reserve Derived from Coronary Imaging and Computational Fluid Dynamics," *Interventional cardiology (London, England),* vol. 9, pp. 145-150, 2014.

[86] N. P. R. Sand, K. T. Veien, S. S. Nielsen, B. L. Nørgaard, P. Larsen, A. Johansen*, et al.*, "Prospective Comparison of FFR Derived From Coronary CT Angiography With SPECT Perfusion Imaging in Stable Coronary Artery Disease," *JACC: Cardiovascular Imaging,* vol. 11, p. 1640, 2018.

[87] A. Coenen, Y.-H. Kim, M. Kruk, C. Tesche, J. D. Geer, A. Kurata*, et al.*, "Diagnostic Accuracy of a Machine-Learning Approach to Coronary Computed Tomographic Angiography–Based Fractional Flow Reserve," *Circulation: Cardiovascular Imaging,* vol. 11, p. e007217, 2018.

[88] N. H. J. Pijls, B. de Bruyne, K. Peels, P. H. van der Voort, H. J. R. M. Bonnier, J. Bartunek*, et al.*, "Measurement of Fractional Flow Reserve to Assess the Functional Severity of Coronary-Artery Stenoses," *New England Journal of Medicine,* vol. 334, pp. 1703-1708, 1996/06/27 1996.

[89] G. Fragiacomo, K. Reck, L. Lorenzen, and E. V. Thomsen, "Novel designs for application specific MEMS pressure sensors," *Sensors (Basel, Switzerland),* vol. 10, pp. 9541-9563, 2010.

[90] F. Stam, H. Kuisma, F. Gao, J. Saarilahti, D. G. Martins, A. Karkkainen*, et al.*, "Integration of a capacitive pressure sensing system into the outer catheter wall for coronary artery FFR measurements," in *Bio-Mems and Medical Microdevices Iii*. vol. 10247, S. VanDenDriesche, I. Giouroudi, and M. DelgadoRestituto, Eds., ed, 2017.

[91] J. Yang, S. Luo, X. Zhou, J. Li, J. Fu, W. Yang*, et al.*, "Flexible, Tunable, and Ultrasensitive Capacitive Pressure Sensor with Microconformal Graphene Electrodes," *ACS Applied Materials & Interfaces,* vol. 11, pp. 14997-15006, 2019/04/24 2019.

[92] F. Stam, H. Kuisma, F. Gao, J. Saarilahti, D. G. Martins, A. Kärkkäinen*, et al.*, *Integration of a capacitive pressure sensing system into the outer catheter wall for coronary artery FFR measurements* vol. 10247: SPIE, 2017.

[93] A. V. Tran, X. Zhang, and B. Zhu, "The Development of a New Piezoresistive Pressure Sensor for Low Pressures," *IEEE Transactions on Industrial Electronics,* vol. 65, pp. 6487-6496, 2018.

[94] T. Kan, H. Takahashi, N. Binh-Khiem, Y. Aoyama, Y. Takei, K. Noda*, et al.*, "Design of a piezoresistive triaxial force sensor probe using the sidewall doping method," *Journal of Micromechanics and Microengineering,* vol. 23, p. 035027, 2013/02/06 2013.

[95] J. Brown Adam, Z. Teng, A. Calvert Patrick, K. Rajani Nikil, O. Hennessy, N. Nerlekar*, et al.*, "Plaque Structural Stress Estimations Improve Prediction of Future Major Adverse Cardiovascular Events After Intracoronary Imaging," *Circulation: Cardiovascular Imaging,* vol. 9, p. e004172, 2016/06/01 2016.

[96] T. Dave, J. Ezhilan, H. Vasnawala, and V. Somani, "Plaque regression and plaque stabilisation in cardiovascular diseases," *Indian journal of endocrinology and metabolism,* vol. 17, pp. 983-989, Nov-Dec 2013.

[97] W.-T. Park, R. K. Kotlanka, L. Lou, M. Hamidullah, and C. Lee, "MEMS tri-axial force sensor with an integrated mechanical stopper for guidewire applications," *Microsystem Technologies,* vol. 19, pp. 1005-1015, 2013/07/01 2013.

[98] G. S. Mintz, S. E. Nissen, W. D. Anderson, S. R. Bailey, R. Erbel, P. J. Fitzgerald*, et al.*, "American College of Cardiology Clinical Expert Consensus Document on Standards for Acquisition, Measurement and Reporting of Intravascular Ultrasound Studies (IVUS) - A report of the American College of Cardiology Task Force on Clinical Expert Consensus - Documents developed in collaboration with the European Society of Cardiology endorsed by the Society of Cardiac Angiography and Interventions," *Journal of the American College of Cardiology,* vol. 37, pp. 1478-1492, Apr 2001.

[99] J. H. Sung and J. S. Jeong, "Development of High-Frequency (>60 MHz) Intravascular Ultrasound (IVUS) Transducer by Using Asymmetric Electrodes for Improved Beam Profile," *Sensors (Basel, Switzerland),* vol. 18, p. 4414, 2018.

[100] M. Su, Z. Zhang, J. Hong, Y. Huang, P. Mu, Y. Yu*, et al.*, "Cable-Shared Dual-Frequency Catheter for Intravascular Ultrasound," *IEEE Transactions on Ultrasonics, Ferroelectrics, and Frequency Control,* vol. 66, pp. 849-856, 2019.
[101] X. Li, J. W. Li, J. Jing, T. Ma, S. S. Liang, J. Zhang*, et al.*, "Integrated IVUS-OCT Imaging for Atherosclerotic Plaque Characterization," *Ieee Journal of Selected Topics in Quantum Electronics,* vol. 20, Mar-Apr 2014.
[102] J. W. Li, T. Ma, J. Jing, J. Zhang, P. M. Patel, K. K. Shung*, et al.*, "Miniature optical coherence tomography-ultrasound probe for automatically coregistered three-dimensional intracoronary imaging with real-time display," *Journal of Biomedical Optics,* vol. 18, Oct 2013.
[103] T. Ma, M. Yu, J. Li, C. E. Munding, Z. Chen, C. Fei*, et al.*, "Multi-frequency intravascular ultrasound (IVUS) imaging," *IEEE transactions on ultrasonics, ferroelectrics, and frequency control,* vol. 62, pp. 97-107, 2015.
[104] F. S. Foster, C. J. Pavlin, K. A. Harasiewicz, D. A. Christopher, and D. H. Turnbull, "Advances in ultrasound biomicroscopy," *Ultrasound in Medicine & Biology,* vol. 26, pp. 1-27, 2000/01/01/ 2000.
[105] C. Fei, C. T. Chiu, X. Chen, Z. Chen, J. Ma, B. Zhu*, et al.*, "Ultrahigh Frequency (100 MHz-300 MHz) Ultrasonic Transducers for Optical Resolution Medical Imagining," *Scientific reports,* vol. 6, pp. 28360-28360, 2016.
[106] X. Li, W. Wu, Y. Chung, W. Y. Shih, W. H. Shih, Q. F. Zhou*, et al.*, "80-MHz Intravascular Ultrasound Transducer Using PMN-PT Free-Standing Film," *Ieee Transactions on Ultrasonics Ferroelectrics and Frequency Control,* vol. 58, pp. 2281-2288, Nov 2011.
[107] X. Li, T. Ma, J. Tian, P. D. Han, Q. F. Zhou, and K. K. Shung, "Micromachined PIN-PMN-PT Crystal Composite Transducer for High-Frequency Intravascular Ultrasound (IVUS) Imaging," *Ieee Transactions on Ultrasonics Ferroelectrics and Frequency Control,* vol. 61, pp. 1171-1178, Jul 2014.
[108] T. Ma, M. Yu, Z. Chen, C. Fei, K. K. Shung, and Q. Zhou, "Multi-frequency intravascular ultrasound (IVUS) imaging," *IEEE Transactions on Ultrasonics, Ferroelectrics, and Frequency Control,* vol. 62, pp. 97-107, 2015.
[109] J. M. Cannata, T. A. Ritter, C. Wo-Hsing, R. H. Silverman, and K. K. Shung, "Design of efficient, broadband single-element (20-80 MHz) ultrasonic transducers for medical imaging applications," *IEEE Transactions on Ultrasonics, Ferroelectrics, and Frequency Control,* vol. 50, pp. 1548-1557, 2003.
[110] W. B. Qiu, Y. Chen, C. M. Wong, B. Q. Liu, J. Y. Dai, and H. R. Zheng, "A novel dual-frequency imaging method for intravascular ultrasound applications," *Ultrasonics,* vol. 57, pp. 31-35, Mar 2015.
[111] K. H. Martin, B. D. Lindsey, J. G. Ma, T. C. Nichols, X. N. Jiang, and P. A. Dayton, "EX VIVO PORCINE ARTERIAL AND CHORIOALLANTOIC MEMBRANE ACOUSTIC ANGIOGRAPHY USING DUAL-FREQUENCY INTRAVASCULAR ULTRASOUND PROBES," *Ultrasound in Medicine and Biology,* vol. 42, pp. 2294-2307, Sep 2016.
[112] J. G. Ma, X. N. Jiang, K. H. Martin, P. A. Dayton, Y. Li, Q. F. Zhou*, et al.*, "Dual Frequency Transducers for Intravascular Ultrasound Super-harmonic Imaging and Acoustic Angiography," in *2014 Ieee International Ultrasonics Symposium*, ed, 2014, pp. 675-678.
[113] X. Ma, P. L. Truong, N. H. Anh, and S. J. Sim, "Single gold nanoplasmonic sensor for clinical cancer diagnosis based on specific interaction between nucleic acids and protein," *Biosensors and Bioelectronics,* vol. 67, pp. 59-65, 2015/05/15/ 2015.
[114] Z. Wang, H. Wenbin, X. Jiang, K. H. Martin, and P. A. Dayton, "Dual-frequency IVUS array for contrast enhanced intravascular ultrasound imaging," in *2015 IEEE International Ultrasonics Symposium (IUS)*, 2015, pp. 1-4.
[115] Z. Wang, K. H. Martin, P. A. Dayton, and X. Jiang, "Real-time ultrasound angiography using superharmonic dual-frequency (2.25MHz/30MHz) cylindrical array: In vitro study," *Ultrasonics,* vol. 82, pp. 298-303, 2018/01/01/ 2018.

[116] A. F. W. V. d. Steen, J. K. Poulsen, E. Cherin, and F. S. Foster, "Harmonic imaging at high frequencies for IVUS," in *1999 IEEE Ultrasonics Symposium. Proceedings. International Symposium (Cat. No.99CH37027)*, 1999, pp. 1537-1540 vol.2.

[117] C. E. Munding, E. Chérin, I. Jourard, J. J. Weyers, D. E. Goertz, B. K. Courtney*, et al.*, "Development of a 3 French Dual-Frequency Intravascular Ultrasound Catheter," *Ultrasound in Medicine & Biology,* vol. 44, pp. 251-266, 2018/01/01/ 2018.

[118] J. P. Kilroy, A. V. Patil, J. J. Rychak, and J. A. Hossack, "An IVUS transducer for microbubble therapies," *IEEE Transactions on Ultrasonics, Ferroelectrics, and Frequency Control,* vol. 61, pp. 441-449, 2014.

[119] M. Abran, B. E. Stähli, N. Merlet, T. Mihalache-Avram, M. Mecteau, E. Rhéaume*, et al.*, "Validating a bimodal intravascular ultrasound (IVUS) and near-infrared fluorescence (NIRF) catheter for atherosclerotic plaque detection in rabbits," *Biomedical optics express,* vol. 6, pp. 3989-3999, 2015.

[120] M. Hoshino, Y. Kanaji, A. Sugano, M. Yamaguchi, M. Hada, Y. Sumino*, et al.*, "PREVALENCE OF THIN CAP FIBROATHEROMA AND PLAQUE RUPTURE IN RELATION TO THE PHYSIOLOGICAL STENOSIS SEVERITY DETERMINED BY FRACTIONAL FLOW RESERVE AND CORONARY FLOW RESERVE," *Journal of the American College of Cardiology,* vol. 73, p. 1123, 2019.

[121] A. Ahmadi, G. W. Stone, J. Leipsic, P. W. Serruys, L. Shaw, H. Hecht*, et al.*, "Association of Coronary Stenosis and Plaque Morphology With Fractional Flow Reserve and OutcomesCoronary Stenosis, Fractional Flow Reserve, and OutcomesCoronary Stenosis, Fractional Flow Reserve, and Outcomes," *JAMA Cardiology,* vol. 1, pp. 350-357, 2016.

[122] C. Ball, G. Pontone, and M. Rabbat, "Fractional Flow Reserve Derived from Coronary Computed Tomography Angiography Datasets: The Next Frontier in Noninvasive Assessment of Coronary Artery Disease," *BioMed research international,* vol. 2018, pp. 2680430-2680430, 2018.

[123] P. Rajiah and C. D. Maroules, "Myocardial ischemia testing with computed tomography: emerging strategies," *Cardiovascular diagnosis and therapy,* vol. 7, pp. 475-488, 2017.

[124] M. T. Lu, M. Ferencik, R. S. Roberts, K. L. Lee, A. Ivanov, E. Adami*, et al.*, "Noninvasive FFR Derived From Coronary CT Angiography: Management and Outcomes in the PROMISE Trial," *JACC. Cardiovascular imaging,* vol. 10, pp. 1350-1358, 2017.

[125] E. Hulten, R. Blankstein, and M. F. Di Carli, "The value of noninvasive computed tomography derived fractional flow reserve in our current approach to the evaluation of coronary artery stenosis," *Current opinion in cardiology,* vol. 31, pp. 970-976, 2016.

[126] J. Leipsic, T.-H. Yang, A. Thompson, B.-K. Koo, G. B. J. Mancini, C. Taylor*, et al.*, "CT Angiography (CTA) and Diagnostic Performance of Noninvasive Fractional Flow Reserve: Results From the Determination of Fractional Flow Reserve by Anatomic CTA (DeFACTO) Study," *American Journal of Roentgenology,* vol. 202, pp. 989-994, 2014/05/01 2014.

[127] I. Streitner, M. Goldhofer, S. Cho, H. Thielecke, R. Kinscherf, F. Streitner*, et al.*, *Electric impedance spectroscopy of human atherosclerotic lesions* vol. 206, 2009.

[128] F. Yu, X. Dai, T. Beebe, and T. Hsiai, "Electrochemical impedance spectroscopy to characterize inflammatory atherosclerotic plaques," *Biosensors & bioelectronics,* vol. 30, pp. 165-173, 2011.

[129] J. Ma, Y. Luo, R. R. Sevag Packard, T. Ma, Y. Ding, P. Abiri*, et al.*, "Ultrasonic Transducer-Guided Electrochemical Impedance Spectroscopy to Assess Lipid-Laden Plaques," *Sensors and actuators. B, Chemical,* vol. 235, pp. 154-161, 2016/11// 2016.